

Article

Thermal Stability and Mechanical Properties of Al-Zn and Al-Bi-Zn Alloys Deformed by ECAP

Hailong Jia ^{1,2}, Yanan Piao ¹, Kaining Zhu ¹, Chaoran Yin ¹, Wenqiang Zhou ¹, Feng Li ³ and Min Zha ^{1,2,*}

¹ Key Laboratory of Automobile Materials of Ministry of Education, College of Materials Science and Engineering, Jilin University, Changchun 130025, China; jihailong@jlu.edu.cn (H.J.); piaoyan20@mails.jlu.edu.cn (Y.P.); zhukn1619@mails.jlu.edu.cn (K.Z.); yincr2219@mails.jlu.edu.cn (C.Y.); zhouwq19@mails.jlu.edu.cn (W.Z.)

² International Center of Future Science, Jilin University, Changchun 130012, China

³ FAW Foundary Co., Ltd., Changchun 130012, China; lifeng_fc@faw.com.cn

* Correspondence: minzha@jlu.edu.cn; Tel.: +86-137-5655-4479

Abstract: It is well known that ultrafine grained and nanocrystalline materials show enhanced strength, while they are susceptible to thermally induced grain coarsening. The present work aims to enhance the thermal stability of ultrafine Al grains produced by equal channel angular pressing (ECAP) via dynamically precipitation. Detailed characterization by electron backscatter diffraction (EBSD) and transmission electron microscopy (TEM) has been carried out to reveal the microstructural evolution during both ECAP and post-ECAP annealing. After five passes of ECAP, both Al-8Zn and Al-6Bi-8Zn alloys show an ultrafine grain structure together with dynamic precipitated nanoscale Zn particles along grain boundaries. Upon annealing at 200 °C, ultrafine grains in the Al-8Zn and Al-6Bi-8Zn alloys show a remarkable thermal stability compared to the Al-8Bi alloy, which is mainly due to the presence of nanoscale Zn precipitates along grain boundaries. The present work reveals that nanoscale Zn particles have a positive effect on preserving the ultrafine grains during annealing, which is useful for the design of UFG Al alloys with improved thermal stability.

Keywords: ultrafine grains; dynamic precipitation; thermal stability; texture; mechanical properties



Citation: Jia, H.; Piao, Y.; Zhu, K.; Yin, C.; Zhou, W.; Li, F.; Zha, M. Thermal Stability and Mechanical Properties of Al-Zn and Al-Bi-Zn Alloys Deformed by ECAP. *Metals* **2021**, *11*, 2043. <https://doi.org/10.3390/met11122043>

Academic Editor: Michael E. Kassner

Received: 13 November 2021

Accepted: 15 December 2021

Published: 16 December 2021

Publisher's Note: MDPI stays neutral with regard to jurisdictional claims in published maps and institutional affiliations.



Copyright: © 2021 by the authors. Licensee MDPI, Basel, Switzerland. This article is an open access article distributed under the terms and conditions of the Creative Commons Attribution (CC BY) license (<https://creativecommons.org/licenses/by/4.0/>).

1. Introduction

Al alloys have received great interest for lightweighting in automobile and aerospace industries due to their high specific strength [1,2]. It is well known that grain refinement is effective in strengthening Al alloys. In recent years, severe plastic deformation (SPD) processes have been developed for producing ultrafine grained (submicrometer) or nanocrystalline Al alloys [3–6] with improved strengths in comparison to their coarse-grained counterparts [3,4,7]. However, a disadvantage of UFG materials is a significant decrease in ductility, which seriously hinders the structural application of UFG materials. The poor ductility is attributed to the low work-hardening rate of the materials, which is a result of the low dislocation accumulation capability of the ultrafine grains [8]. In general, a suitable annealing treatment can lead to better ductility for wrought Al alloys. Thus, annealing on SPD-processed materials has been extensively studied to optimize its strength and ductility [3].

However, enhanced grain coarsening rates of SPD-processed microstructures have been observed during the early stage of annealing, which have been attributed to the faster boundary mobility of non-equilibrium GBs [9,10]. This is a major deficiency of many SPD-processed UFG alloys, such as equal channel angular pressing (ECAP) [11], and thermally stable microstructures are of particular importance for the application of UFG alloys. Therefore, how to hinder recrystallization and rapid grain growth effectively in Al alloys at elevated temperatures is worth investigating.

It is well known that the presence of a dispersion of fine secondary phase particles has a huge influence on recrystallization and grain growth. Most studies focus on the

grain refinement mechanism and dynamic precipitation during ECAP [12–16]. However, the effect of dynamically precipitated Zn phase in Al-Zn alloys on the grain structure evolution during annealing is less investigated. Moreover, the pinning effect of nano-sized particles on ECAP texture evolution during post-ECAP annealing is less investigated as well. Therefore, the present work was initiated to systematically study the microstructure and texture evolution of ECAP-processed Al-8Zn and Al-6Bi-8Zn alloys upon annealing. In particular, the effect of fine Zn precipitates pre-existing before annealing on grain coarsening has been investigated. The results of the present work will be useful for expanding the potential application of UFG Al alloys.

2. Materials and Methods

The Al-8Zn and Al-6Bi-8Zn (wt. %) alloys were produced by melting commercial purity Al, Zn, and Bi, using an electric resistance furnace at 720 °C. Square cross-section bars with dimensions of 100 mm × 19.5 mm × 19.5 mm were machined from the as-cast ingots. These bars were coated with a thin layer of a graphite lubricant and then deformed by a 90° ECAP die (Figure 1a) via route Bc at room temperature (RT). Route Bc means a 90° rotation around the longitudinal (ED) axis of the ECAP bar between each pass, which has been proved to be effective in the formation of homogeneous equiaxed grain structures with a large fraction of high angle boundaries [17–19]. The samples were processed for various numbers of passes through the die, i.e., 1 pass, 3 passes, and 5 passes. For convenience, the deformed samples after *X* passes of ECAP are referred to as *XP* samples. Following ECAP, post-ECAP isothermal annealing at 200 °C was performed on the 1P, 3P, and 5P samples using an oil furnace for various times, i.e., 2 h, 8 h, and 96 h. After annealing, as-deformed samples were immediately water quenched to RT.

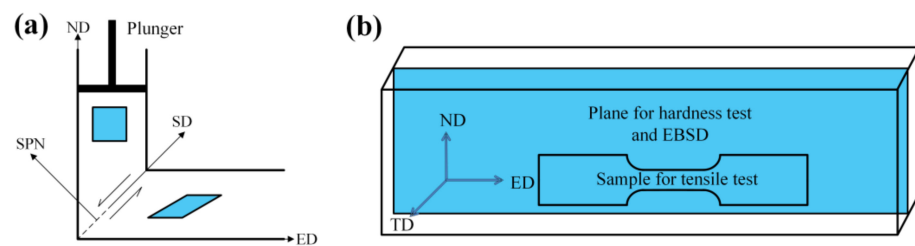


Figure 1. (a) Sketch of the ECAP die, showing the shear direction (SD), shear plane normal (SPN), and (b) EBSD, hardness, and tensile test measurement planes (ED-ND) with reference to the ECAP die geometry.

Microstructures of the cast, deformed, and annealed samples were characterized by backscattered electron (BSE, Zeiss Ultra 55, Oberkochen, Germany) imaging, electron backscatter diffraction (EBSD, Nordif, Trondheim, Norway), and transmission electron microscopy (TEM, JEOL Ltd., Tokyo, Japan) on ED-ND planes (Figure 1b). Here, ED and ND are abbreviations for the extrusion direction and the normal direction, respectively. Samples for EBSD were prepared by standard metallographic techniques followed by ion milling at 3.5 V for 30 min (at a tilt angle of $\approx 70^\circ$, and with a gas flow rate of ≈ 0.08 mL/min) using a Hitachi IM 3000 ion milling machine (Hitachi, Tokyo, Japan). EBSD was carried out using a Hitachi SU-6600 field emission gun SEM (FEG-SEM, Hitachi Ltd., Tokyo, Japan) equipped with a Nordif EBSD detector and the TSL OIM software (OIM 7.2, EDAX Inc., Mahwah, NJ, USA). TEM foils were prepared by twin-jet electro polishing in a solution of 33% nitric acid-methanol at -30 °C. TEM imaging was performed using the JEOL 2100 TEM at 200 kV. In the present work, texture analysis was conducted based on the data obtained from EBSD.

The hardness was measured by applying a load of 5 kg for 15 s, using a DKV-1S Vickers hardness testing machine (Matsuzawa, Akita, Japan). The hardness value was averaged from six indentations. For each condition, uniaxial tensile testing was performed on 3 samples with a gauge length of 5 mm and thickness of ≈ 2 mm at room temperature under

a strain rate of $5 \times 10^{-4} \text{ s}^{-1}$, using a MTS 810 hydraulic universal testing machine (MTS, Eden Prairie, MN, USA) a 100 kN capacity and a video extensometer (TRV, SHIMADZU, Kyoto, Japan).

3. Results and Discussion

3.1. Microstructure Evolution

3.1.1. As-Cast Microstructure

As shown in Figure 2, both the as-cast Al-8Zn and Al-6Bi-8Zn alloys are with an equiaxed α -Al grain structure, $\approx 50 \mu\text{m}$ for both of these two alloys. From Figure 2b, no Zn precipitates in the as-cast Al-8Zn sample can be observed. For the as-cast Al-6Bi-8Zn alloy, the area fraction and the average size of Bi particles were measured to be $\approx 1.2\%$ and $\approx 5 \mu\text{m}$, respectively.

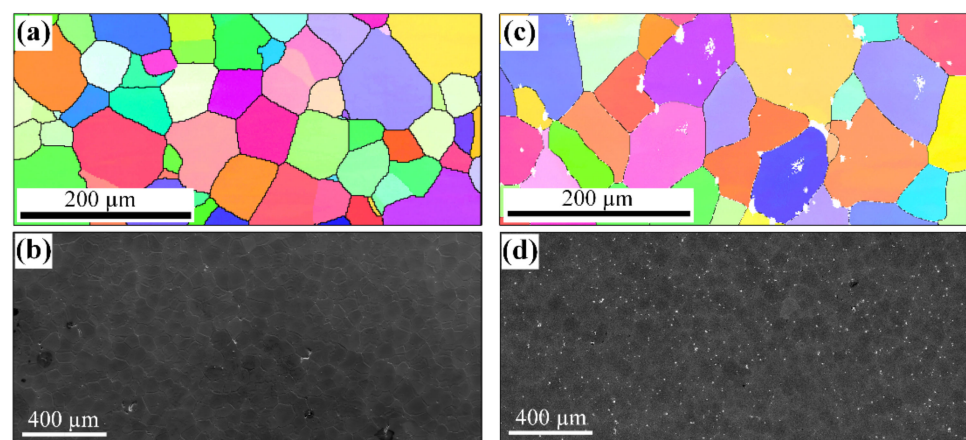


Figure 2. Microstructures of the as-cast Al-8Zn (a,b) and Al-6Bi-8Zn (c,d) alloys. (a,c) EBSD-IPF maps, (b,d) SEM-BSE images.

3.1.2. Deformation Microstructure after ECAP

Figure 3 shows microstructures of the ECAP-deformed 5P Al-8Zn and Al-6Bi-8Zn alloys. As displayed in Figure 3a,b, ultrafine grains are obtained in both alloys via continuous dynamic recrystallization (CDRX), since equiaxed fine (sub)grains are surrounded by high-angle boundary (HAB) segments connected to low-angle boundary (LAB) segments. The average grain size (equivalent diameter) of the 5P Al-6Bi-8Zn sample ($\approx 0.5 \mu\text{m}$) is smaller than that of the 5P Al-8Zn sample ($\approx 0.9 \mu\text{m}$) due to the presence of Bi particles [5]. As shown in Figure 3c,d, the dislocation density is much lower, and GBs are relatively well-defined, with interiors of some grains even free of dislocations. It indicates that massive dislocation annihilations and rearrangement have occurred during ECAP deformation. As can be seen from STEM images in Figure 3e,f, a large amount of nano-sized Zn particles distributed mainly along HABs have formed in both alloys as a result of dynamic precipitation [20]. The average size and number density of Zn particles are 80 nm and $5 \times 10^{12} \text{ m}^{-2}$ in the 5P Al-6Bi-8Zn alloy, which are larger than that of the 5P Al-8Zn alloy (the average size and number density of Zn particles are 40 nm and $3 \times 10^{12} \text{ m}^{-2}$, respectively).

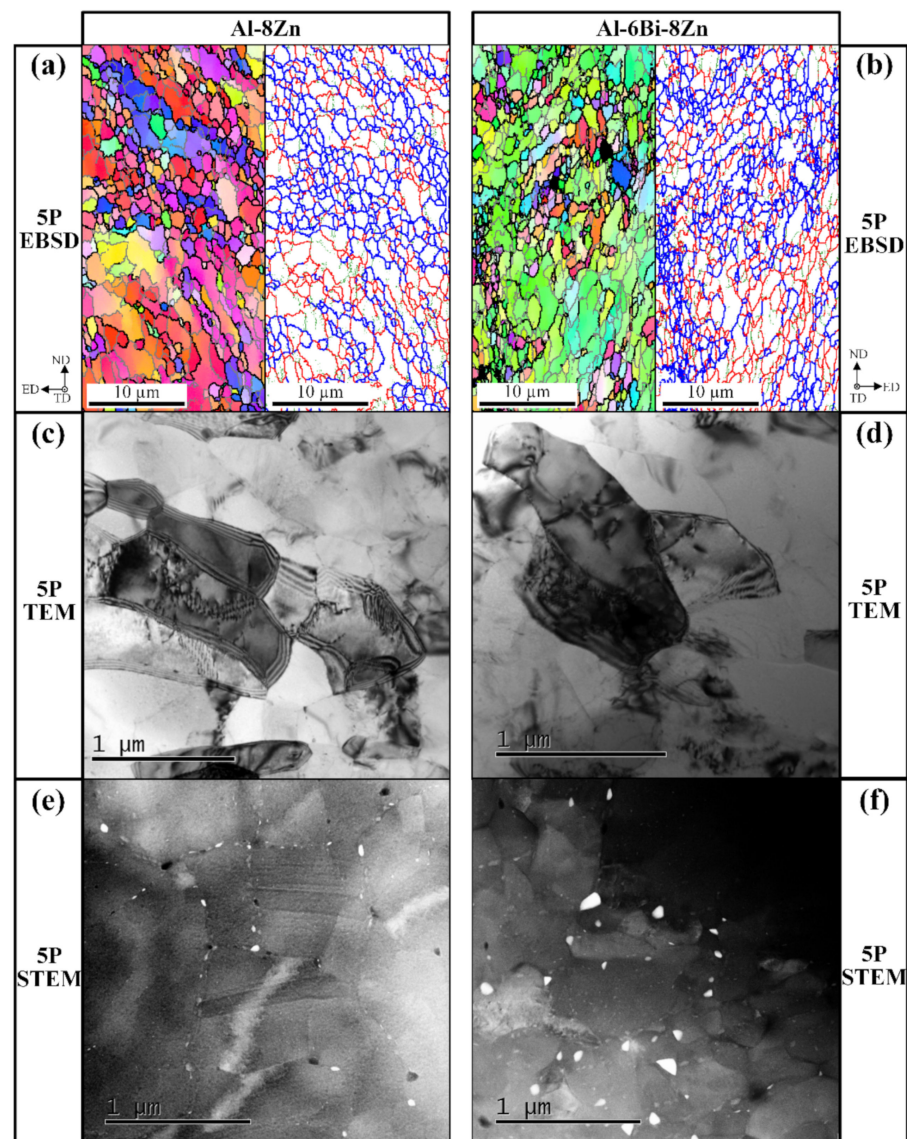


Figure 3. Microstructures of the 5P Al-8Zn and Al-6Bi-8Zn alloys. (a,b) EBSD, (c,d) TEM, and (e,f) STEM. In boundary maps, green, red, and blue lines depict boundaries with misorientations in the range of $2^\circ \leq \theta < 5^\circ$, $5^\circ \leq \theta < 15^\circ$ and $15^\circ \leq \theta < 180^\circ$, respectively.

3.1.3. Microstructural Evolution during Post-ECAP Annealing

Figure 4 depicts microstructural evolution during post-ECAP annealing. In our previous work, it has been proved that soft Bi particles can promote CDRX during ECAP [5], which has occurred to such an extent that the influence of coarse Bi particles on the particle simulated nucleation (PSN) mechanism is rather limited during post-ECAP annealing. After annealing at 200 °C for 2 h, no obvious grain growth can be observed (Figure 4a,b), indicating that the migration of HABs between the deformed grains is rather limited. Thus, only the recovery process takes place in the structure, i.e., thermally activated annihilation and rearrangement of dislocations. It is well known that UFG alloys produced by SPD are inherently unstable at elevated temperatures. In another study [21], when the ECAP deformed Al-8Bi alloy was annealed at 200 °C for 5 min, partial discontinuous recrystallization occurred rapidly; i.e., most grains grow rapidly (larger than 25 μm) and only a few fine grains retained locally along boundaries of coarse recrystallized grains. It demonstrates that in the present work, the grain structures of ECAP-deformed Al-8Zn and Al-6Bi-8Zn alloys are much more stable than that of the ECAP-processed Al-8Bi alloy in the work [21].

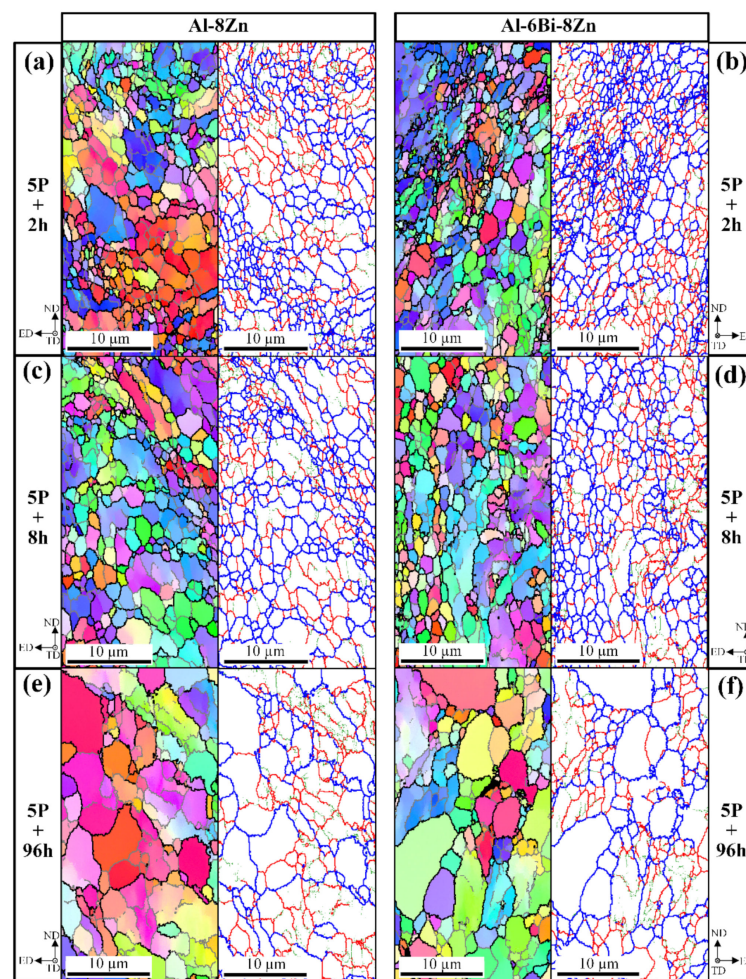


Figure 4. EBSD IPF maps and boundary maps of the annealed (at 200 °C) Al-8Zn and Al-6Bi-8Zn alloys. (a,b) 2 h, (c,d) 8 h, and (e,f) 96 h. In boundary maps, green, red, and blue lines depict boundaries with misorientations in the range of $2^\circ \leq \theta < 5^\circ$, $5^\circ \leq \theta < 15^\circ$, and $15^\circ \leq \theta < 180^\circ$, respectively.

As can be seen from Figure 4c,d, with further increasing the annealing time to 8 h, the number density of ultrafine grains (with grain sizes less than 1 μm) shows a decreasing trend. The evolution of the average grain size (with boundary misorientations larger than 5°) of the 5P and annealed 5P alloys derived from EBSD results are plotted in Figure 5. As can be seen from Figure 5, after annealing time to 8 h, the average grain size becomes larger, which indicates grain coarsening. For the ECAP-deformed Al-8Bi alloy annealed at 200 °C for 8 h [21], the deformation grain structure is consumed almost completely by equiaxed recrystallized grains delineated by HABs ($>50 \mu\text{m}$). It shows a much faster grain coarsening rate than the ECAP deformed Al-8Zn and Al-6Bi-8Zn alloys in the present work. After annealing for 96 h (Figure 4e,f), the grain size distribution becomes heterogeneous, and the average grain sizes of the 5P Al-Zn and Al-Bi-Zn samples increase to 2.3 and 2.2 μm , respectively (Figure 5). The number density of grains with dimensions larger than 10 μm increases, which means that some grains grow faster than others and consume the smaller ones.

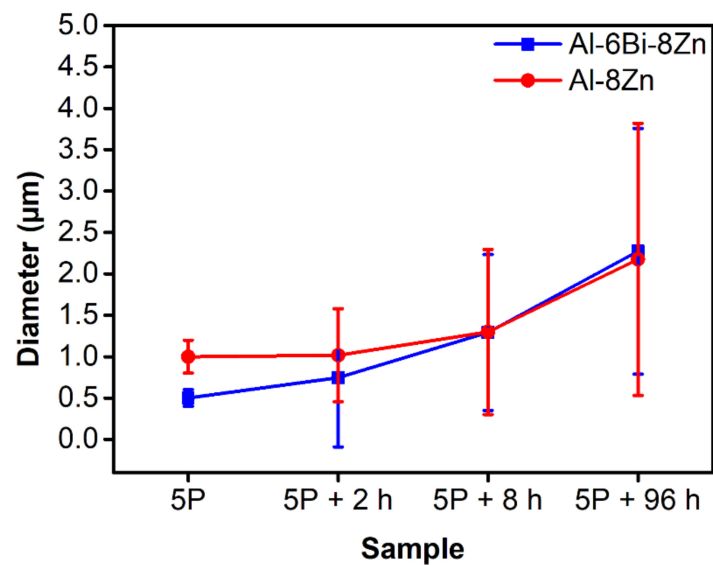


Figure 5. The evolution of average grain size for the as-deformed and annealed (at 200 °C) Al-8Zn and Al-6Bi-8Zn alloys.

Therefore, the present work demonstrates that compared with binary Al-Bi alloys processed by ECAP, the grain structure of ECAP-deformed Al-6Bi-8Zn alloy is very stable at 200 °C, at least up to 8 h. The slow grain coarsening in the present work can be mainly related to the presence of nano-sized Zn particles dynamically formed along GBs during ECAP, which can effectively impede grain boundary migration during long-term annealing by the Zener pinning effect [22]. As a result, the thermal stability of 5P Al-8Zn and 5P Al-6Bi-8Zn alloys is improved. This strategy has never been reported in improving the thermo-stability of UFG Al-Bi based alloys, which shows great practical and industrial potential.

3.2. Texture Evolution

As can be seen from Figure 6a,b, the grain orientation distributions of the 1P samples are nearly centro-symmetric, showing characteristics of the ideal (pure shear) ECAP texture of FCC metals and alloys processed through a 90° ECAP die [23]. Compared to the 1P samples, the texture components of the 3P Al-8Zn and Al-6Bi-8Zn samples become more concentrated with the maximum intensity increased to ≈ 9.1 and 7.8 *mr*, respectively. With increasing ECAP passes to five, the loss of monoclinic symmetry and deviation from ideal positions occurs, which can be related to the formation of ultrafine grains as a result of CDRX. However, the similarity between textures of Al-8Zn and Al-6Bi-8Zn samples demonstrates that CDRX can only modify the ECAP texture in some extent. The effect of annealing at 200 °C on the texture of Al-8Zn and Al-6Bi-8Zn alloys is illustrated in Figure 7. A comparison of Figures 6 and 7 shows that after annealing for 8 h, annealing at 200 °C is not radical enough to eliminate ECAP textures, which further confirms that the grain structures of 5P Al-8Zn and Al-6Bi-8Zn alloys are stable during annealing.

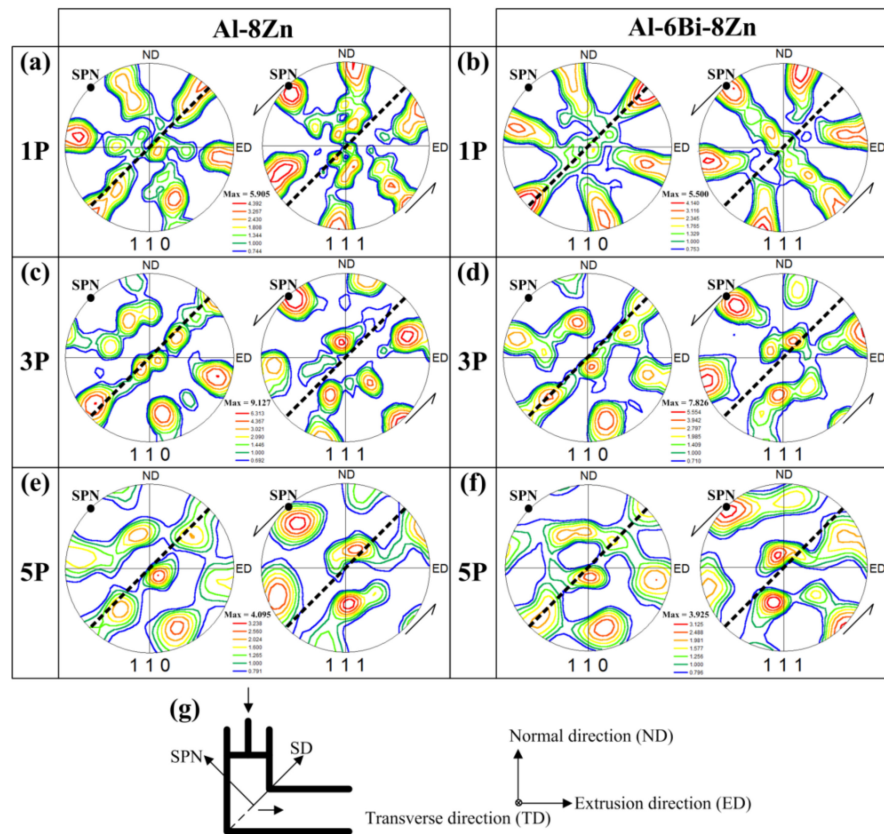


Figure 6. $\{1\ 1\ 0\}$ and $\{1\ 1\ 1\}$ pole figures of ECAP-processed Al-8Zn and Al-6Bi-8Zn alloys. (a) and (b) 1P, (c) and (d) 3P, (e) and (f) 5P, and (g) is a schematic of the ECAP die and its relevant coordinate system. The dotted lines in the pole figures indicate the ideal shear plane (SD and SPN are abbreviations for shear plane and shear plane normal).

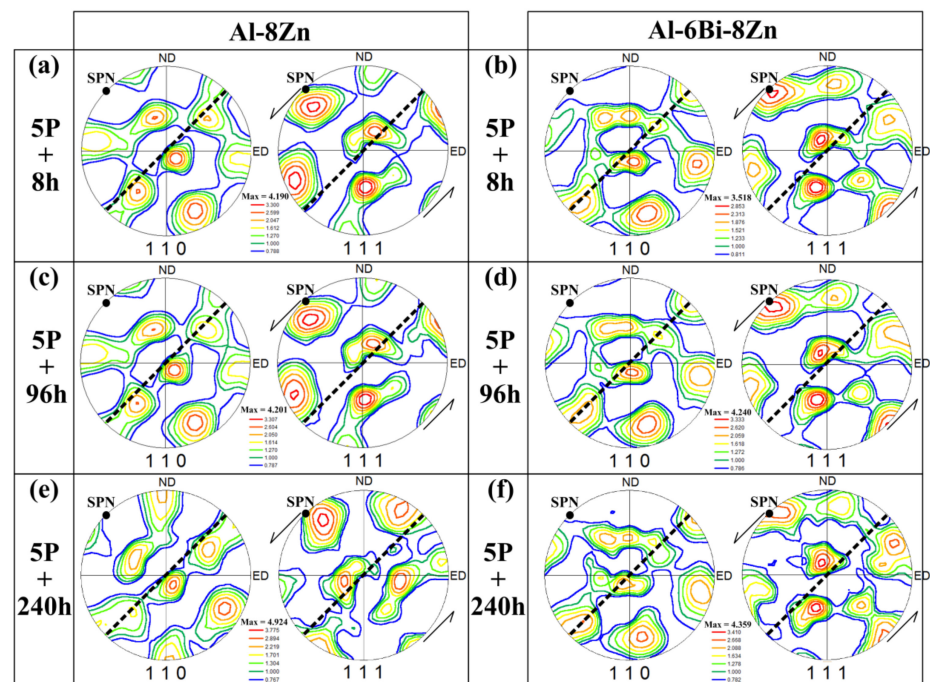


Figure 7. $\{1\ 1\ 0\}$ and $\{1\ 1\ 1\}$ pole figures of ECAP-processed (a–c) Al-8Zn alloy and (d–f) Al-6Bi-8Zn alloy. The dotted lines indicate the ideal shear plane, and SPN is the shear plane normal.

3.3. Mechanical Properties

The evolution of Vickers hardness upon annealing at 200 °C as a function of time is shown in Figure 8. The 5P Al-8Zn and Al-6Bi-8Zn alloys before annealing have a hardness of 66 HV and 73 HV, respectively. Overall, the hardness continuously decreases with increasing the annealing time. In the present work, after annealing for 1 min, the decreased hardness is caused by thermally activated annihilation and rearrangement of dislocations. The decrease in the hardness of the 5P Al-6Bi-8Zn alloy is larger than that of the 5P Al-8Zn alloy. This can be mainly attributed to the faster occurrence of recovery in the 5P Al-6Bi-8Zn alloy due to the smaller grain size. After annealing for 1 h, the Vickers hardness of the Al-8Zn and the Al-6Bi-8Zn alloy is much higher than that of the ECAP-deformed commercial purity (99.5%) Al alloy (≈ 42 HV) after annealing at 200 °C for 1 h [24].

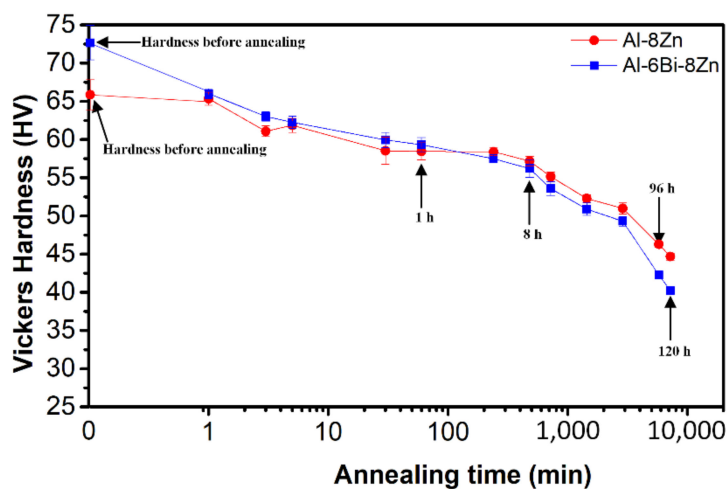


Figure 8. Evolution of Vickers hardness of the 5P Al-8Zn and Al-6Bi-8Zn alloys as a function of annealing time at 200 °C.

With increasing the annealing time up to 8 h, the decrease in hardness is rather slow and gradual, which is consistent with the microstructural evolution. After annealing for 120 h, the hardness of the Al-8Zn and Al-6Bi-8Zn alloys drops down to ≈ 43.7 HV and ≈ 40.7 HV, respectively. The lower hardness of the Al-6Bi-8Zn alloy should be due to the presence of soft Bi particles. The significant decrease in hardness is mainly attributed to grain growth. Compared to their as-cast counterparts, the hardness of these two alloys is still higher.

As shown in Figure 9, tensile tests were conducted on the 5P Al-8Zn and Al-6Bi-8Zn alloys after annealing for 96 h. For comparison, the tensile results of the as-cast and as-deformed 5P samples are also given in Figure 9, and the corresponding tensile properties are given in Table 1. It is apparent that for both alloys, five passes of ECAP can lead to a substantial increase in yield strength and ultimate tensile strength, with a decline in ductility. The improvement of yield strength after five passes of ECAP compared to the as-cast state is a result of increased grain boundary strengthening (≈ 96 MPa) and dislocation strengthening (≈ 49 MPa), coupled with decreased solid solution strengthening [5]. The low uniform elongation is related to the very limited work-hardening potential [5]. The tensile fracture morphologies of the 5P Al-8Zn and Al-6Bi-8Zn samples are shown in Figure 10. It can be seen that the 5P Al-8Zn sample exhibits more and deeper dimples than the 5P Al-6Bi-8Zn sample, indicating that the 5P Al-8Zn sample is more ductile. The flake-shaped Bi particles in the 5P Al-6Bi-8Zn sample cause decohesion of the Bi particle/matrix interfaces, which leads to poor ductility.

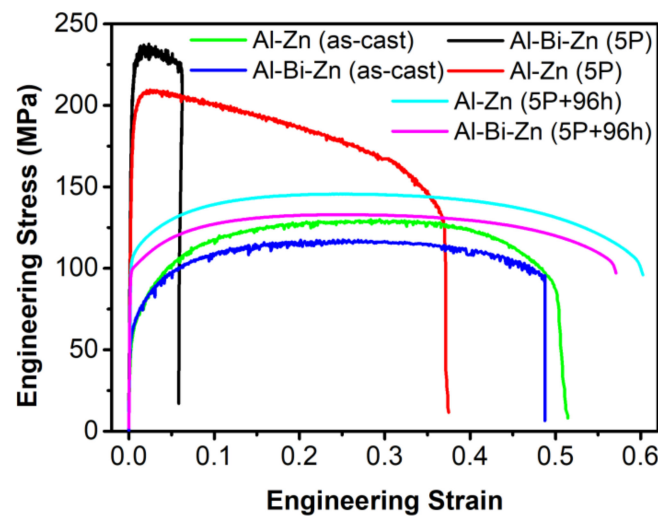


Figure 9. Tensile engineering stress–strain curves of the Al-8Zn and Al-6Bi-8Zn alloys.

Table 1. Tensile properties of the as-cast, as-deformed, and annealed Al-8Zn and Al-6Bi-8Zn alloys.

Material (wt. %)	Yield Strength (YS) (0.2% Offset) [MPa]	Ultimate Tensile Stress (UTS) [MPa]	Uniform Elongation (UE) [%]	Elongation to Failure (EF) [%]
Al-8Zn (as-cast)	66 ± 2	130 ± 4	26.0 ± 0.5	51.5 ± 1
Al-8Zn (5P)	199 ± 4	221 ± 5	2.2 ± 0.2	37.5 ± 0.6
Al-8Zn (5P + 96 h)	106 ± 2	146 ± 3	24.6 ± 0.4	60.3 ± 0.3
Al-6Bi-8Zn (as-cast)	63 ± 3	118 ± 3	22.0 ± 0.3	48.4 ± 0.8
Al-6Bi-8Zn (5P)	211 ± 4	238 ± 4	2.3 ± 0.2	6.0 ± 0.3
Al-8Zn (as-cast)	99 ± 2	133 ± 3	24.8 ± 0.3	57.2 ± 0.4
Al-8Zn (as-cast)	66 ± 2	130 ± 4	26.0 ± 0.5	51.5 ± 1

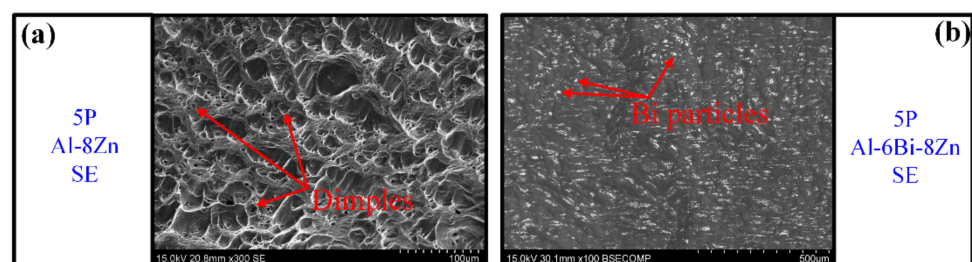


Figure 10. Fracture morphologies. (a) SE images of the 5P Al-8Zn sample, (b) BSE image of the 5P Al-6Bi-8Zn sample.

Compared to the 5P Al-8Zn and Al-6Bi-8Zn alloys, the yield strength is considerably reduced by annealing at 200 °C for 96 h. Nevertheless, it can be seen that post-ECAP annealing is very advantageous in improving the ductility of the ECAP processed Al-8Zn and Al-6Bi-8Zn alloys. The uniform elongation is increased significantly, ≈ 11 times as large as the 5P samples. In addition, the yield strength of the 5P + 96h Al-8Zn alloy is ≈ 7 MPa higher than that of the 5P + 96h Al-6Bi-8Zn alloy. Since the average grain size of these alloys are nearly the same, the decreased yield strength of the 5P + 96h Al-6Bi-8Zn sample can be due to the presence of coarse soft Bi particles.

Furthermore, the yield strength of the 5P + 96 h samples is ≈ 1.6 times of its as-cast counterparts, with higher values of elongation to failure as well, which can be ascribed to the fine dislocation-free grains. On the one hand, the fine grains can contribute larger grain boundary strengthening, making the yield strength higher. On the other hand, fine

grain structures make deformation more homogeneous, which can prevent early crack nucleation due to strain localization and is beneficial for elongation to failure [25].

4. Conclusions

The present work aims to produce UFG Al alloys with stable ultrafine grain structures by adding Zn, in which the effect of nano-sized Zn particles on ECAP texture evolution during post-ECAP annealing has also been investigated. The main conclusions are summarized as follows:

- (1) Only recovery occurs upon annealing at ≈ 200 °C for 2 h, while the coarsening of UFG grains are depressed. In contrast to severely deformed commercial purity Al and the binary Al-8Bi alloys, the present 5P Al-8Zn and Al-6Bi-8Zn alloys show a more stable thermal stability. It can be mainly ascribed to the retarded GB migration due to the Zener pinning effect of pre-existing fine Zn particles dynamically precipitated along GBs.
- (2) ECAP texture of the 5P Al-8Zn and Al-6Bi-8Zn alloys remain stable upon annealing at 200 as a result of the stable grain structure.
- (3) Annealing at 200 °C leads to a reduction in the strength of 5P Al-8Zn and Al-6Bi-8Zn alloys, while the uniform elongations are much improved, reaching $\approx 24.6\%$ and $\approx 24.8\%$, respectively.

Author Contributions: Conceptualization, H.J. and Y.P.; methodology, H.J., Y.P., K.Z., C.Y., W.Z. and F.L.; writing—original draft preparation, H.J. and Y.P.; writing—review and editing, H.J. and M.Z.; supervision, H.J.; funding acquisition, H.J. and M.Z. All authors have read and agreed to the published version of the manuscript.

Funding: This research was funded by the National key research and development program, grant number 2019YFB2006501; the Natural Science Foundation of China, grant number 52001133 and 51871108; and the Science and Technology Development Program of Jilin Province, grant number 20210201115GX and 20200201193JC.

Institutional Review Board Statement: Not applicable.

Informed Consent Statement: Not applicable.

Data Availability Statement: The data presented in this study are available on request from the corresponding author. The data are not publicly available due to technical or time limitations.

Conflicts of Interest: The authors declare no conflict of interest.

References

1. Dursun, T.; Soutis, C. Recent developments in advanced aircraft aluminium alloys. *Mater. Design* **2014**, *56*, 862–871. [[CrossRef](#)]
2. Aryshenskii, E.V.; Hirsch, J.; Konovalov, S.V.; Prah, U. Specific Features of Microstructural Evolution During Hot Rolling of the As-Cast Magnesium-Rich Aluminum Alloys with Added Transition Metal Elements. *Metall. Mater. Trans. A* **2019**, *50*, 5782–5799. [[CrossRef](#)]
3. Jia, H.L.; Bjørge, R.; Cao, L.F.; Song, H.; Marthinsen, K.; Li, Y.J. Quantifying the grain boundary segregation strengthening induced by post-ECAP aging in an Al-5Cu alloy. *Acta Mater.* **2018**, *155*, 199–213. [[CrossRef](#)]
4. Jia, H.L.; Bjørge, R.; Marthinsen, K.; Li, Y.J. The deformation and work hardening behaviour of a SPD processed Al-5Cu alloy. *J. Alloys Compd.* **2017**, *697*, 239–248. [[CrossRef](#)]
5. Jia, H.L.; Bjørge, R.; Marthinsen, K.; Mathiesen, R.H.; Li, Y.J. Soft particles assisted grain refinement and strengthening of an Al-Bi-Zn alloy subjected to ECAP. *Mater. Sci. Eng. A* **2017**, *703*, 304–313. [[CrossRef](#)]
6. Kaibyshev, R.; Shipilova, K.; Musin, F.; Motohashi, Y. Continuous dynamic recrystallization in an Al-Li-Mg-Sc alloy during equal-channel angular extrusion. *Mater. Sci. Eng. A* **2005**, *396*, 341–351. [[CrossRef](#)]
7. Zhang, Y.; Jin, S.; Trimby, P.W.; Liao, X.; Murashkin, M.Y.; Valiev, R.Z.; Liu, J.; Cairney, J.M.; Ringer, S.P.; Sha, G. Dynamic precipitation, segregation and strengthening of an Al-Zn-Mg-Cu alloy (AA7075) processed by high-pressure torsion. *Acta Mater.* **2019**, *162*, 19–32. [[CrossRef](#)]
8. Gil Sevillano, J.; Aldazabal, J. Ductilization of nanocrystalline materials for structural applications. *Scr. Mater.* **2004**, *51*, 795–800. [[CrossRef](#)]
9. Lian, J.; Valiev, R.Z.; Baudalet, B. On the enhanced grain growth in ultrafine grained metals. *Acta Metall. Mater.* **1995**, *43*, 4165–4170. [[CrossRef](#)]

10. Wang, J.; Iwahashi, Y.; Horita, Z.; Furukawa, M.; Nemoto, M.; Valiev, R.Z.; Langdon, T.G. An investigation of microstructural stability in an Al-Mg alloy with submicrometer grain size. *Acta Mater.* **1996**, *44*, 2973–2982. [[CrossRef](#)]
11. Karelin, R.D.; Khmelevskaya, I.Y.; Komarov, V.S.; Andreev, V.A.; Perkas, M.M.; Yusupov, V.S.; Prokoshkin, S.D. Effect of Quasi-Continuous Equal-Channel Angular Pressing on Structure and Properties of Ti-Ni Shape Memory Alloys. *J. Mater. Eng. Perform.* **2021**, *30*, 3096–3106. [[CrossRef](#)]
12. Jia, H.L.; Marthinsen, K.; Li, Y.J. Effect of soft Bi particles on grain refinement during severe plastic deformation. *Trans. Nonferr. Met. Soc. China* **2017**, *27*, 971–976. [[CrossRef](#)]
13. Iwahashi, Y.; Wang, J.; Horita, Z.; Nemoto, M.; Langdon, T.G. Principle of equal-channel angular pressing for the processing of ultra-fine grained materials. *Scr. Mater.* **1996**, *35*, 143–146. [[CrossRef](#)]
14. Furukawa, M.; Iwahashi, Y.; Horita, Z.; Nemoto, M.; Langdon, T.G. The shearing characteristics associated with equal-channel angular pressing. *Mater. Sci. Eng. A* **1998**, *257*, 328–332. [[CrossRef](#)]
15. Iwahashi, Y.; Horita, Z.; Nemoto, M.; Langdon, T.G. An investigation of microstructural evolution during equal-channel angular pressing. *Acta Mater.* **1997**, *45*, 4733–4741. [[CrossRef](#)]
16. Iwahashi, Y.; Horita, Z.; Nemoto, M.; Langdon, T.G. The process of grain refinement in equal-channel angular pressing. *Acta Mater.* **1998**, *46*, 3317–3331. [[CrossRef](#)]
17. Valiev, R.Z.; Langdon, T.G. Principles of equal-channel angular pressing as a processing tool for grain refinement. *Prog. Mater. Sci.* **2006**, *51*, 881–981. [[CrossRef](#)]
18. Shaeri, M.H.; Shaeri, M.; Ebrahimi, M.; Salehi, M.T.; Seyyedain, S.H. Effect of ECAP temperature on microstructure and mechanical properties of Al-Zn-Mg-Cu alloy. *Prog. Nat. Sci.* **2016**, *26*, 182–191. [[CrossRef](#)]
19. Shaeri, M.H.; Salehi, M.T.; Seyyedain, S.H.; Abutalebi, M.R.; Park, J.K. Characterization of microstructure and deformation texture during equal channel Angular pressing of Al-Zn-Mg-Cu alloy. *J. Alloys Compd.* **2013**, *576*, 350–357. [[CrossRef](#)]
20. Muñoz-Morris, M.A.; Gutierrez-Urrutia, I.; Morris, D.G. Effect of equal channel angular pressing on strength and ductility of Al-TiAl composites. *Mater. Sci. Eng. A* **2005**, *396*, 3–10. [[CrossRef](#)]
21. Zha, M.; Yu, Z.Y.; Qian, F.; Wang, H.Y.; Li, Y.J.; Mathiesen, R.H.; Roven, H.J. Achieving dispersed fine soft Bi particles and grain refinement in a hypermonotectic Al-Bi alloy by severe plastic deformation and annealing. *Scr. Mater.* **2018**, *155*, 124–128. [[CrossRef](#)]
22. Humphreys, F.J.; Hatherly, M. *Recrystallization and Related Annealing Phenomena*; Elsevier: Amsterdam, The Netherlands, 2004.
23. Li, S.; Beyerlein, I.J.; Bourke, M.A.M. Texture formation during equal channel angular extrusion of fcc and bcc materials: Comparison with simple shear. *Mater. Sci. Eng. A* **2005**, *394*, 66–77. [[CrossRef](#)]
24. Bowen, J.R. Strength and structure in commercial purity aluminium after large strain. *Mater. Sci. Eng. A* **2008**, *483–484*, 231–234. [[CrossRef](#)]
25. Zheng, L.J.; Chen, C.Q.; Zhou, T.T.; Liu, P.Y.; Zeng, M.G. Structure and properties of ultrafine-grained Al-Zn-Mg-Cu and Al-Cu-Mg-Mn alloys fabricated by ECA pressing combined with thermal treatment. *Mater. Charact.* **2002**, *49*, 455–461. [[CrossRef](#)]